Research Paper
J. Astron. Space Sci. 32(4), 379-386 (2015)
http://dx.doi.org/10.5140/JASS.2015.32.4.379

JASS Journal of Astronomy and Space Sciences

Fuel-Optimal Altitude Maintenance of Low-Earth-Orbit Spacecrafts by Combined Direct/Indirect Optimization

Kyung-Ha Kim, Chandeok Park†, Sang-Young Park
Astrodynamics and Control Laboratory, Department of Astronomy, Yonsei University, Seoul 03722, Korea

This work presents fuel-optimal altitude maintenance of Low-Earth-Orbit (LEO) spacecrafts experiencing non-negligible air drag and *J*2 perturbation. A pseudospectral (direct) method is first applied to roughly estimate an optimal fuel consumption strategy, which is employed as an initial guess to precisely determine itself. Based on the physical specifications of KOrea Multi-Purpose SATellite-2 (KOMPSAT-2), a Korean artificial satellite, numerical simulations show that a satellite ascends with full thrust at the early stage of the maneuver period and then descends with null thrust. While the thrust profile is presumably bang-off, it is difficult to precisely determine the switching time by using a pseudospectral method only. This is expected, since the optimal switching epoch does not coincide with one of the collocation points prescribed by the pseudospectral method, in general. As an attempt to precisely determine the switching time and the associated optimal thrust history, a shooting (indirect) method is then employed with the initial guess being obtained through the pseudospectral method. This hybrid process allows the determination of the optimal fuel consumption for LEO spacecrafts and their thrust profiles efficiently and precisely.

Keywords: altitude maintenance, direct/indirect optimization, fuel optimization, pseudospectral method, shooting method

1. INTRODUCTION

Operating an Earth-observing satellite at sufficiently lower altitudes can improve its spatial resolution and help a satellite sensor identify smaller details of ground objects. While QuickBird, a typical high-resolution commercial Earth-observing satellite owned by DigitalGlobe, collects the panchromatic imagery at a resolution of 61 cm and an altitude of 450 km, KOrea Multi-Purpose SATellite-2 (KOMPSAT-2) in a 685 km sun-synchronous orbit has a resolution of 1m (Kim 2013). If KOMPSAT-2 were able to observe the ground object at a lower altitude, it could have distinguished more details with a better resolution. However, with the lowering of the operating altitude of a satellite and without a proper altitude maintenance management, the atmospheric drag becomes stronger to ultimately cause its reentry into the Earth. Therefore, for the altitude maintenance of Low-Earth-Orbit (LEO) spacecrafts, fuel-optimal strategy becomes highly critical, as it saves cost and extends the lifetime of the mission as well.

Park et al.(2007) analyzed the effect of drag on orbital variations of KOMPSAT-1 during strong solar and geomagnetic activities. Halbach(2000) presented a numerical study of an optimal periodic thrusting method for LEO spacecrafts using the Legendre-Gauss-Lobatto (LGL) pseudospectral collocation codes developed at Naval Postgraduate School. Park et al.(2008) studied the amount of fuel required to maintain a very low-Earth-orbit with severe air drag using a collocation method. These studies considered air drag as the only perturbation force and acquired solutions using a direct collocation method. However, the actual motion of such satellites in real environments is also affected by other gravitational and non-gravitational perturbations owing to the irregular shape of the Earth (Jo et al. 2011).

In this study, the *J*2 perturbation, which has significant effect on LEO spacecrafts, is considered along with air

Received Sep 23, 2015 **Revised** Nov 24, 2015 **Accepted** Nov 26, 2015
†**Corresponding Author**
E-mail: park.chandeok@yonsei.ac.kr, ORCID: 0000-0002-1616-6780
Tel: +82-2-2123-5692, Fax: +82-2-392-7680

drag. Also, both a pseudospectral (direct) and a shooting (indirect) method are used together to improve the accuracy of optimization results obtained from previous studies. For numerical simulations, the physical characteristics of KOMPSAT-2, a Korean satellite, are used, and the atmospheric density model from Ionospheric Prediction Service (IPS) Radio and Space Services (Kennewell 1999) is used to reflect highly dominant air density variation caused by solar activity.

The rest of this paper is organized as follows. Section 2 formally presents a fuel-optimal altitude maintenance problem including the objective function, and the governing equations of motion and equality/inequality constraints. Necessary conditions for optimality, such as the costate equations and the transversality conditions are also derived for the indirect optimization method. Section 3 proposes the key process for combining the direct and indirect methods. Section 4 presents simulation results of fuel optimization under various circumstances and the corresponding analyses. Finally, the last section presents the conclusions drawn from the study.

2. PROBLEM FORMULATION

2.1 Altitude Maintenance Problem

First, an objective function to minimize the fuel consumption is defined as

$$J = \int_0^{t_f} |T| dt \tag{1}$$

where, t_f is the terminal time and $|T|$ is the thrust magnitude. The objective function is subject to the equations of motion of a satellite:

$$\begin{aligned}
\dot{x} &= v_x \\
\dot{y} &= v_y \\
\dot{z} &= v_z \\
\dot{v}_x &= -\mu\frac{x}{r^3} + \frac{T_x}{m} - \frac{1}{2}\frac{C_D A}{m}\rho|v|v_x - \frac{3J_2\mu R_\oplus^2 x}{2r^5}\left(1-\frac{5z^2}{r^2}\right) \\
\dot{v}_y &= -\mu\frac{y}{r^3} + \frac{T_y}{m} - \frac{1}{2}\frac{C_D A}{m}\rho|v|v_y - \frac{3J_2\mu R_\oplus^2 y}{2r^5}\left(1-\frac{5z^2}{r^2}\right) \\
\dot{v}_z &= -\mu\frac{z}{r^3} + \frac{T_z}{m} - \frac{1}{2}\frac{C_D A}{m}\rho|v|v_z - \frac{3J_2\mu R_\oplus^2 z}{2r^5}\left(3-\frac{5z^2}{r^2}\right) \\
\dot{m} &= -\frac{T}{v_e}
\end{aligned} \tag{2}$$

The set of equations under Eq. (2) governs the motion of a spacecraft under the influence of its own thrust, central gravity, J_2 perturbation and atmospheric drag. (x, y, z) are the position components, (v_x, v_y, v_z) are the associated velocity components, and m is the mass of a spacecraft; $r=\sqrt{x^2+y^2+z^2}$ is the magnitude of position vector of a spacecraft and $v=\sqrt{v_x^2+v_y^2+v_z^2}$ is the magnitude of velocity vector; the thrust components are expressed as $(T_x, T_y, T_z)=(T\cos\beta\cos\alpha, T\cos\beta\sin\alpha, T\cos\beta)$, where $\alpha\in[0,2\pi]$ and $\beta\in[-\pi/2, \pi/2]$ represent the longitudinal and latitudinal steering angles, respectively (Fig. 1); v_e is the exhaust velocity; ρ is the atmospheric density; C_D is the drag coefficient, and A is the cross-sectional area of a spacecraft; μ is the gravitational parameter of the Earth, J_2 is the oblateness factor, and $R_\oplus$ is the mean radius of the Earth.

For altitude maintenance, a lower limit is imposed on the altitude as an inequality constraint:

$$r(t) - r_{ref} \geq 0 \tag{3}$$

where, r_{ref} is the radius of the reference orbit. In addition, the capacity of a thruster is imposed as an inequality constraint:

$$0 \leq |T(t)| \leq T_{max} \tag{4}$$

where, T_{max} is the maximum thrust. The spacecraft is assumed to be initially located on the x-axis at the initial time without loss of generality and to have a circular velocity at the corresponding altitude:

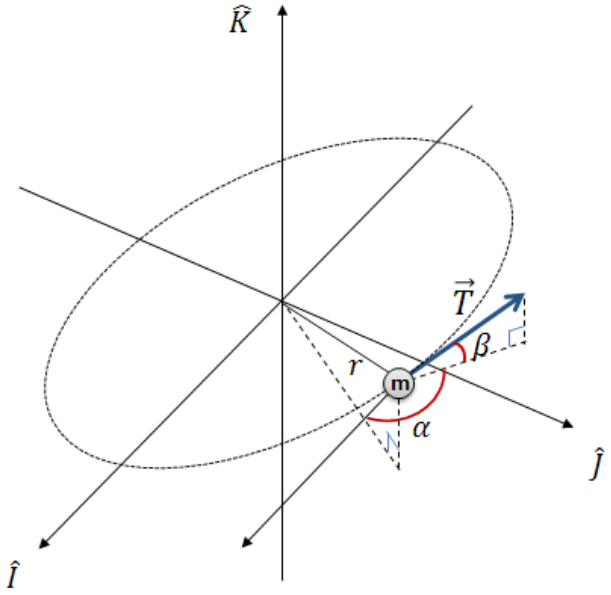

Fig. 1. Longitudinal and latitudinal steering angles.

$$\begin{cases} x(0)=r_0 \\ y(0)=0 \\ z(0)=0 \\ v_x(0)=0 \\ v_y(0)=v_0 \\ v_z(0)=0 \\ m(0)=m_0 \end{cases} \tag{5}$$

where, r_0 is the initial radius, v_0 is the initial circular speed, and m_0 is the initial mass. Next, for computational efficiency, all the physical variables are scaled using canonical units; the radius of the reference orbit and the time it takes a spacecraft to move 1 radian in the reference orbit are used as Distance Unit (DU) and Time Unit (TU), respectively. Then, the normalized equations of motion are expressed as follows (Kim 2014):

$$\begin{aligned} \dot{\bar{x}} &= \bar{v}_x \\ \dot{\bar{y}} &= \bar{v}_y \\ \dot{\bar{z}} &= \bar{v}_z \\ \dot{\bar{v}}_x &= -\frac{\bar{x}}{\bar{r}^3}+\frac{\bar{T}_x}{\bar{m}}-\frac{1}{2}\frac{C_D A}{\bar{m}}\rho\left(\frac{r_{ref}}{m_{ref}}\right)\bar{v}\,\bar{v}_x-\frac{3J_2R_\oplus^2}{2r_{ref}^2}\frac{\bar{x}}{\bar{r}^5}\left(1-\frac{5\bar{z}^2}{\bar{r}^2}\right) \\ \dot{\bar{v}}_y &= -\frac{\bar{y}}{\bar{r}^3}+\frac{\bar{T}_y}{\bar{m}}-\frac{1}{2}\frac{C_D A}{\bar{m}}\rho\left(\frac{r_{ref}}{m_{ref}}\right)\bar{v}\,\bar{v}_y-\frac{3J_2R_\oplus^2}{2r_{ref}^2}\frac{\bar{y}}{\bar{r}^5}\left(1-\frac{5\bar{z}^2}{\bar{r}^2}\right) \\ \dot{\bar{v}}_z &= -\frac{\bar{z}}{\bar{r}^3}+\frac{\bar{T}_z}{\bar{m}}-\frac{1}{2}\frac{C_D A}{\bar{m}}\rho\left(\frac{r_{ref}}{m_{ref}}\right)\bar{v}\,\bar{v}_z-\frac{3J_2R_\oplus^2}{2r_{ref}^2}\frac{\bar{z}}{\bar{r}^5}\left(3-\frac{5\bar{z}^2}{\bar{r}^2}\right) \\ \dot{\bar{m}} &= -\frac{\bar{T}}{\left(v_e/v_{ref}\right)} \end{aligned} \tag{6}$$

where, v_{ref} is the circular speed and m_{ref} is the initial mass(m_0). Note that the bar symbol($\bar{\ }$) represents the normalized variables. Constraints on the radius and thrust magnitude are also normalized as

$$\bar{r}(\bar{t})-1\geq 0 \tag{7}$$

$$0\leq\left|\bar{T}\right|\leq T_{\max}/T_{ref} \tag{8}$$

Here, T_{ref} is the centrifugal force at r_{ref}. If the spacecraft is in the reference orbit at the initial time, the initial boundary conditions are normalized as follows:

$$\begin{cases} \bar{x}(0)=1 \\ \bar{y}(0)=0 \\ \bar{z}(0)=0 \\ \bar{v}_x(0)=0 \\ \bar{v}_y(0)=1 \\ \bar{v}_z(0)=0 \\ \bar{m}(0)=1 \end{cases} \tag{9}$$

2.2 Necessary Conditions for Optimality

To apply the indirect method, the 1st-order necessary conditions for optimality should be derived. In this case, Eqs. (10) and (11) are used instead of Eqs. (1) and (7), respectively, for simplicity in derivation.

$$J=-\bar{m}\left(\bar{t}_f\right) \tag{10}$$

$$\vec{\psi}\left(\vec{x}\left(\bar{t}_f\right),\bar{t}_f\right)=\begin{bmatrix} 1-\bar{x}\left(\bar{t}_f\right)^2-\bar{y}\left(\bar{t}_f\right)^2-\bar{z}\left(\bar{t}_f\right)^2 \\ 1-\bar{v}_x\left(\bar{t}_f\right)^2-\bar{v}_y\left(\bar{t}_f\right)^2-\bar{v}_z\left(\bar{t}_f\right)^2 \end{bmatrix} \tag{11}$$

The Hamiltonian is first defined as

$$\begin{aligned} H=&\left(\lambda_x\bar{v}_x+\lambda_y\bar{v}_y+\lambda_z\bar{v}_z\right)-\frac{1}{\bar{r}^3}\left(\lambda_{vx}\bar{x}+\lambda_{vy}\bar{y}+\lambda_{vz}\bar{z}\right) \\ &-\frac{1}{2}\frac{C_D A}{\bar{m}}\rho\left(\frac{r_{ref}}{m_{ref}}\right)\left|\vec{\bar{v}}\right|\left(\lambda_{vx}\bar{v}_x+\lambda_{vy}\bar{v}_y+\lambda_{vz}\bar{v}_z\right) \\ &+\frac{\bar{T}}{\bar{m}}\left(\lambda_{vx}\cos\beta\cos\alpha+\lambda_{vy}\cos\beta\sin\alpha+\lambda_{vz}\sin\beta\right)-\lambda_m\frac{\bar{T}}{\left(v_e/v_{ref}\right)} \\ &-\frac{3J_2R_\oplus^2}{2r_{ref}^2\bar{r}^5}\left[\lambda_{vx}\bar{x}\left(1-\frac{5\bar{z}^2}{\bar{r}^2}\right)+\lambda_{vy}\bar{y}\left(1-\frac{5\bar{z}^2}{\bar{r}^2}\right)+\lambda_{vz}\bar{z}\left(3-\frac{5\bar{z}^2}{\bar{r}^2}\right)\right] \end{aligned} \tag{12}$$

Here, (λ_x, λ_y, λ_z), (λ_{vx}, λ_{vy}, λ_{vz}), and λ_m are the costates adjoint to the position components, the velocity components, and mass, respectively. The steering angle vector $\vec{u}$ is defined as

$$\vec{u}=\left[cos\beta\cos\alpha\ cos\beta\sin\alpha\ sin\beta\right]^T \tag{13}$$

The optimal longitudinal and latitudinal steering can be obtained from the first-order optimality conditions $\partial H/\partial\alpha=0$, $\partial H/\partial\beta=0$ (Park 2013):

$$\tan\alpha=\frac{\lambda_{vy}}{\lambda_{vx}} \quad\Rightarrow\quad \sin\alpha=-\frac{\lambda_{vy}}{\sqrt{\lambda_{vx}^2+\lambda_{vy}^2}},\ \cos\alpha=-\frac{\lambda_{vx}}{\sqrt{\lambda_{vx}^2+\lambda_{vy}^2}} \tag{14}$$

$$\tan\beta=-\frac{\lambda_{vz}}{\sqrt{\lambda_{vx}^2+\lambda_{vy}^2}} \quad\Rightarrow\quad \sin\beta=-\frac{\lambda_{vz}}{\sqrt{\lambda_{vx}^2+\lambda_{vy}^2+\lambda_{vz}^2}},\ \cos\beta=\frac{\sqrt{\lambda_{vx}^2+\lambda_{vy}^2}}{\sqrt{\lambda_{vx}^2+\lambda_{vy}^2+\lambda_{vz}^2}} \tag{15}$$

Note that the (-) sign of the sine and cosine in Eq. (14) comes from the second-order convexity condition $\partial^2H/\partial\alpha^2\geq 0$ (Kluever & Pierson 1995). Substituting (14) and (15) into the definition of the steering angle vector reveals that $\vec{u}$ is the anti-parallel unit vector to the costate vector adjoint to velocity:

$$\vec{u}=-\frac{\vec{\lambda}_v}{\sqrt{\vec{\lambda}_v^{\mathrm{T}}\vec{\lambda}_v}} \tag{16}$$

Then, the costate equations are derived from $\dot{\lambda}_{(\cdot)}=-\partial H/\partial(\cdot)$, where $(\cdot)$ represents a general state variable (Kim 2014):

$$
\begin{aligned}
\dot{\lambda}_x &= \frac{\lambda_{vx}}{\bar{r}^3} - \frac{3\bar{x}}{\bar{r}^5}\vec{\lambda}_v^T\vec{\bar{r}} + \frac{1}{2}\frac{C_D A}{\bar{m}}\frac{\partial\rho}{\partial\bar{x}}\left(\frac{r_{ref}}{m_{ref}}\right)\left|\vec{\bar{v}}\right|\vec{\lambda}_v^T\vec{\bar{v}} \\
&\quad + \frac{3J_2R_\oplus^2}{2r_{ref}^2}\left[\frac{1}{\bar{r}^5}\left(\lambda_{vx}\left(1-\frac{5\bar{z}^2}{\bar{r}^2}\right)+\frac{10\bar{z}^2\bar{x}}{\bar{r}^2}\vec{\lambda}_v^T\vec{\bar{r}}\right)\right] \\
&\quad + \frac{3J_2R_\oplus^2}{2r_{ref}^2}\left[-\frac{5\bar{x}}{\bar{r}^7}\left(\lambda_{vx}\bar{x}\left(1-\frac{5\bar{z}^2}{\bar{r}^2}\right)+\lambda_{vy}\bar{y}\left(1-\frac{5\bar{z}^2}{\bar{r}^2}\right)+\lambda_{vz}\bar{z}\left(3-\frac{5\bar{z}^2}{\bar{r}^2}\right)\right)\right] \\
\dot{\lambda}_y &= \frac{\lambda_{vy}}{\bar{r}^3} - \frac{3\bar{y}}{\bar{r}^5}\vec{\lambda}_v^T\vec{\bar{r}} + \frac{1}{2}\frac{C_D A}{\bar{m}}\frac{\partial\rho}{\partial\bar{y}}\left(\frac{r_{ref}}{m_{ref}}\right)\left|\vec{\bar{v}}\right|\vec{\lambda}_v^T\vec{\bar{v}} \\
&\quad + \frac{3J_2R_\oplus^2}{2r_{ref}^2}\left[\frac{1}{\bar{r}^5}\left(\lambda_{vy}\left(1-\frac{5\bar{z}^2}{\bar{r}^2}\right)+\frac{10\bar{z}^2\bar{y}}{\bar{r}^2}\vec{\lambda}_v^T\vec{\bar{r}}\right)\right] \\
&\quad + \frac{3J_2R_\oplus^2}{2r_{ref}^2}\left[-\frac{5\bar{y}}{\bar{r}^7}\left(\lambda_{vx}\bar{x}\left(1-\frac{5\bar{z}^2}{\bar{r}^2}\right)+\lambda_{vy}\bar{y}\left(1-\frac{5\bar{z}^2}{\bar{r}^2}\right)+\lambda_{vz}\bar{z}\left(3-\frac{5\bar{z}^2}{\bar{r}^2}\right)\right)\right] \\
\dot{\lambda}_z &= \frac{\lambda_{vz}}{\bar{r}^3} - \frac{3\bar{z}}{\bar{r}^5}\vec{\lambda}_v^T\vec{\bar{r}} + \frac{1}{2}\frac{C_D A}{\bar{m}}\frac{\partial\rho}{\partial\bar{z}}\left(\frac{r_{ref}}{m_{ref}}\right)\left|\vec{\bar{v}}\right|\vec{\lambda}_v^T\vec{\bar{v}} \\
&\quad + \frac{3J_2R_\oplus^2}{2r_{ref}^2}\left[\frac{1}{\bar{r}^5}\left(\lambda_{vz}\left(3-\frac{5\bar{z}^2}{\bar{r}^2}\right)+\frac{10\bar{z}^2}{\bar{r}^2}\vec{\lambda}_v^T\vec{\bar{r}}\left(\bar{z}-1\right)\right)\right] \\
&\quad + \frac{3J_2R_\oplus^2}{2r_{ref}^2}\left[-\frac{5\bar{z}}{\bar{r}^7}\left(\lambda_{vx}\bar{x}\left(1-\frac{5\bar{z}^2}{\bar{r}^2}\right)+\lambda_{vy}\bar{y}\left(1-\frac{5\bar{z}^2}{\bar{r}^2}\right)+\lambda_{vz}\bar{z}\left(3-\frac{5\bar{z}^2}{\bar{r}^2}\right)\right)\right] \\
\dot{\lambda}_{vx} &= -\lambda_x + \frac{1}{2}\frac{C_D A}{\bar{m}}\rho\left(\frac{r_{ref}}{m_{ref}}\right)\left|\vec{\bar{v}}\right|\left(\lambda_{vx}+\frac{v_x}{\left|\vec{\bar{v}}\right|^2}\vec{\lambda}_v^T\vec{\bar{v}}\right) \\
\dot{\lambda}_{vy} &= -\lambda_y + \frac{1}{2}\frac{C_D A}{\bar{m}}\rho\left(\frac{r_{ref}}{m_{ref}}\right)\left|\vec{\bar{v}}\right|\left(\lambda_{vy}+\frac{v_y}{\left|\vec{\bar{v}}\right|^2}\vec{\lambda}_v^T\vec{\bar{v}}\right) \\
\dot{\lambda}_{vz} &= -\lambda_z + \frac{1}{2}\frac{C_D A}{\bar{m}}\rho\left(\frac{r_{ref}}{m_{ref}}\right)\left|\vec{\bar{v}}\right|\left(\lambda_{vz}+\frac{v_z}{\left|\vec{\bar{v}}\right|^2}\vec{\lambda}_v^T\vec{\bar{v}}\right) \\
\dot{\lambda}_m &= -\frac{1}{\bar{m}}\left[\frac{\bar{T}}{\bar{m}}\vec{\lambda}_v^{\mathrm{T}}\vec{\lambda}_v + \frac{1}{2}\frac{C_D A}{\bar{m}}\rho\left(\frac{r_{ref}}{m_{ref}}\right)\left|\vec{\bar{v}}\right|\vec{\lambda}_v^T\vec{\bar{v}}\right]
\end{aligned}
\tag{17}
$$

Finally, the transversality conditions are derived as

$$
\begin{aligned}
\lambda_x\left(\bar{t}_f\right)\bar{y}\left(\bar{t}_f\right) &= \lambda_y\left(\bar{t}_f\right)\bar{x}\left(\bar{t}_f\right) \\
\lambda_y\left(\bar{t}_f\right)\bar{z}\left(\bar{t}_f\right) &= \lambda_z\left(\bar{t}_f\right)\bar{y}\left(\bar{t}_f\right) \\
\lambda_{vx}\left(\bar{t}_f\right)\bar{v}_y\left(\bar{t}_f\right) &= \lambda_{vy}\left(\bar{t}_f\right)\bar{v}_x\left(\bar{t}_f\right) \\
\lambda_{vy}\left(\bar{t}_f\right)\bar{v}_z\left(\bar{t}_f\right) &= \lambda_{vz}\left(\bar{t}_f\right)\bar{v}_y\left(\bar{t}_f\right) \\
\lambda_m\left(\bar{t}_f\right) &= -1
\end{aligned}
\tag{18}
$$

3. ALTITUDE MAINTENANCE ALGORITHM

In general, a direct method is less sensitive to the initial guess, but shows slow convergence and is not highly accurate. An indirect method converges fast with a proper initial guess of costates, but it is difficult to estimate the initial costates themselves. Given the objective function, governing equation, and associated equality/inequality constraints, the optimal fuel consumption and associated thrust profile are calculated using both pseudospectral (direct) and shooting (indirect) methods. In this manner, a hybrid approach combining the direct and indirect methods is proposed.

In a pseudospectral method, the state and control variables are approximated at predetermined collocation points (Halbach 2000). In this study, LGL points are used for the discretization of the system, and Lagrange polynomials are used as trial functions (Elnagar et al. 1995). Fig. 2 shows the flowchart of fuel optimization algorithm based on the pseudospectral method (Kim 2014). The input values are the number of LGL points, information of an assigned orbit, physical specifications of a spacecraft and its thruster, and indices associated with air density. In this method, the states and control guesses at the LGL points should be provided. The differentiation matrix (D_{jk}), LGL points (t_k), and weights (w_k) are determined via a subroutine (lglpoints) (Elnagar et al. 1995). Then, the states and control variables satisfying the constraints while minimizing the objective function are calculated through the 'fmincon' in the optimization Toolbox of MATLAB. The 'fmincon' attempts to find a constrained minimum of a scalar function of multiple variables starting at an initial estimate (MathWorks 2015a).

Fig. 3 shows the time history of altitude and thrust profile after applying the pseudospectral method to the fuel-optimal altitude maintenance problem. A spacecraft first ascends with full thrust at the early stage and then descends with null thrust. While the thrust profile is similar to bang-off, it is difficult to precisely determine the switching time by using a pseudospectral method only. This is expected because the optimal switching epoch does not generally coincide with one of the prescribed collocation points of

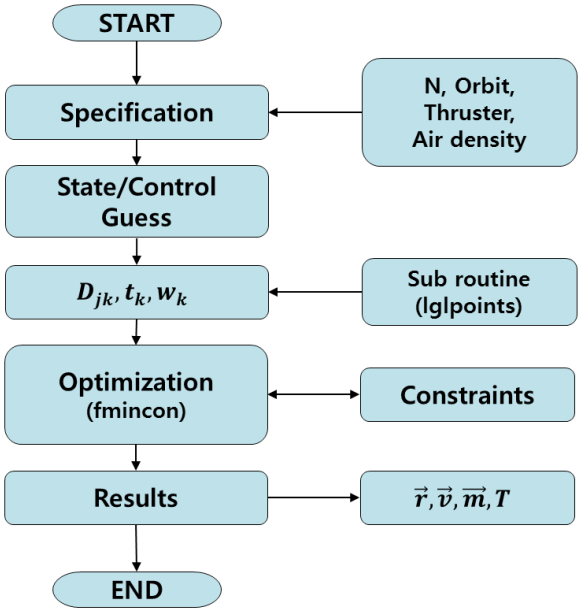

Fig. 2. Flowchart for fuel optimization using a pseudospectral method.

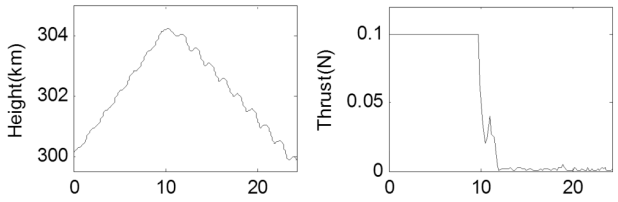

Fig. 3. Results of fuel optimization using a pseudospectral method.

the pseudospectral method. As an attempt to precisely determine the switching time and its associated optimal thrust history, a shooting method is employed with its initial guess obtained from the solution of the pseudospectral method. Fig. 4 shows the flowchart of a fuel optimization algorithm based on a shooting method. Pontryagin's principle (Pontryagin 1987) yields an optimality strategy for thrust magnitude $\bar{T}$:

$$\bar{T}^* = \arg\min_{\bar{T}} H = \begin{cases} T_{\max} / T_{ref}, & \text{if } S < 0 \\ 0, & \text{if } S > 0 \\ \text{singular}, & \text{if } S = 0 \end{cases} \tag{19}$$

Here, S stands for the switching function defined as

$$S \equiv -\left(\frac{\sqrt{\vec{\lambda}_v \cdot \vec{\lambda}_v}}{\bar{m}} + \frac{v_{ref}}{ve} \cdot \lambda_m \right) \tag{20}$$

When S has a value near '0', it is difficult to numerically define its sign. In order to prevent this numerical obscurity, the switching epoch is estimated on the basis of the time history of simulation results using a pseudospectral method. Then, the guess of switching epoch (t_s) is used instead of S for determining $\bar{T}$, as follows:

$$\bar{T}^*(\bar{t}) = \arg\min_{\bar{T}} H(\bar{t}) = \begin{cases} T_{\max} / T_{ref}, & \text{if } \bar{t} < t_s \\ 0, & \text{if } \bar{t} > t_s \\ \text{singular}, & \text{if } \bar{t} = t_s \end{cases} \tag{21}$$

The process of updating the initial guesses is iterated until the transversality conditions are satisfied, and this process of solving nonlinear algebraic equations is performed using the MATLAB built-in function, 'fsolve'. The 'fsolve' finds a root (zero) of a system of nonlinear equations (MathWorks 2015b).

4. SIMULATION RESULTS AND DISCUSSIONS

In the altitude maintenance scenario, the assigned altitude is 300 km and a spacecraft starts on the assigned

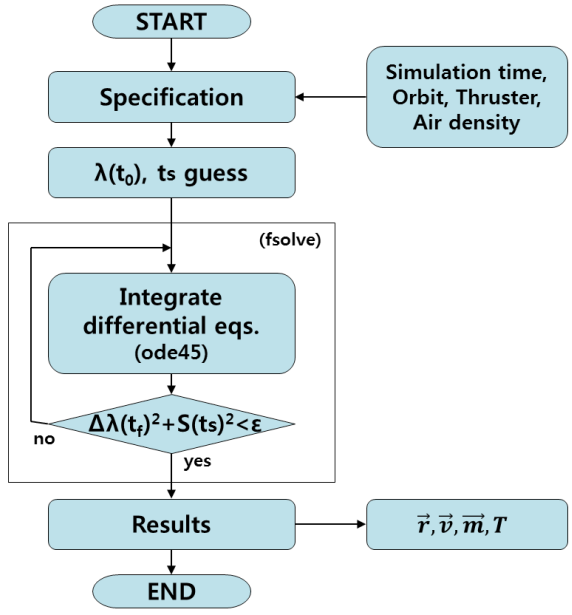

Fig. 4. Flowchart for fuel optimization using a shooting method.

Table 1. Specifications of satellite and its thruster

Satellite	**Mass**	**Cross-Sectional Area**	**Drag Coefficient**
	800 kg	13.6 m^2	3.4
Thruster	**Max. Thrust**		**Specific impulse**
	0.1 N		224 s

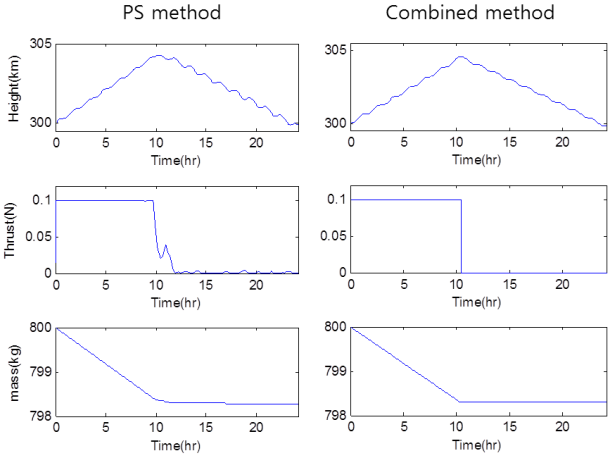

Fig. 5. Results of fuel optimization (time histories of altitude, thrust, and mass) using pseudospectral (left) and combined (right) methods.

altitude with circular velocity. The physical characteristics of the spacecraft (KOMPSAT-2) and the specifications of the thruster are presented in Table 1.

Fig. 5 and Table 2 show that the obscure switching time obtained using the pseudospectral method is precisely determined by applying the shooting method. From the time history of the pseudospectral method, the switching time could be guessed within the range of 9–11 hr. Table 3 shows

Table 2. Comparison between results of pseudospectral and combined methods

Optimization Method	PS	Combined
Fuel Consumption (kg)	1.730	1.718
Peak Altitude (km)	304.256	304.574
Final Altitude (km)	299.899	299.861
Switching Time (hr)	-	10.488

Table 3. Simulation results of pseudospectral method with switching time guess

Switching Time Guess (hr)	5	20
Fuel Consumption (kg)	0.751	3.071
Peak Altitude (km)	301.917	308.543
Final Altitude (km)	294.529	306.621
Switching Time (hr)	4.581	18.742

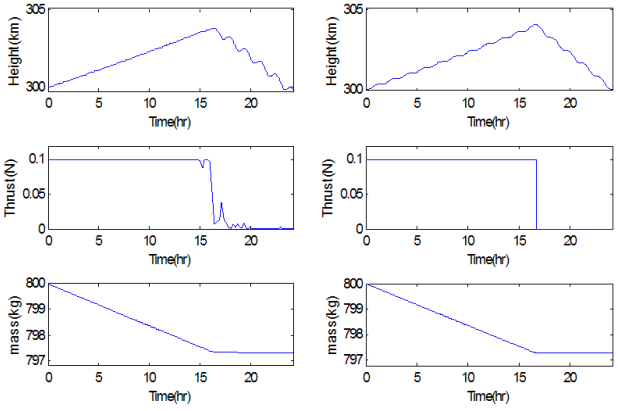

Fig. 6. Simulation results for maximum solar activity using pseudospectral (left) and combined (right) methods.

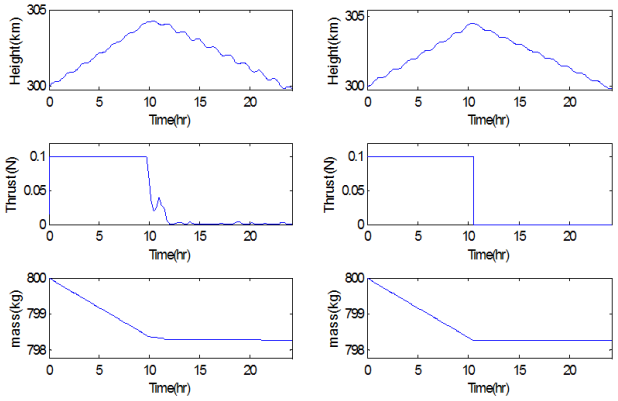

Fig. 7. Simulation results for mean solar ativity using pseudospectral (left) and combined (right) methods.

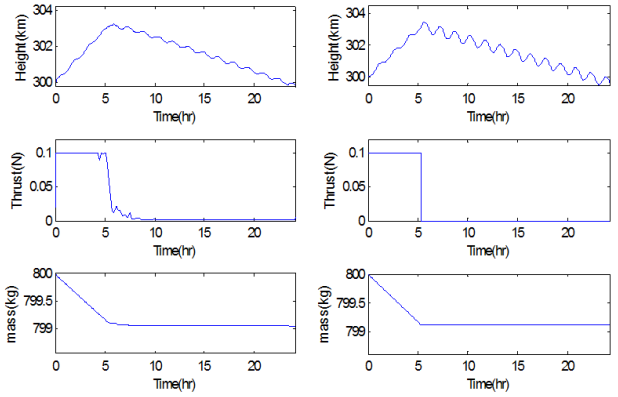

Fig. 8. Simulation results for minimum solar activity using pseudospectral (left) and combined (right) methods.

that a guess selected within this range leads to a proper (local) optimal solution satisfying the altitude maintenance constraints. In contrast, if the guess of switching time is (deliberately) selected outside this range, a non-compatible solution without satisfying the given altitude constraint is generated. This implies that the proposed combined approach can be effectively used for this type of numerically sensitive problems.

Figs. 6–8 show optimization results with different atmospheric densities (caused by solar activity) using the pseudospectral and combined methods in which the atmospheric model offered by the Australian IPS Radiation & Space Services is implemented (Kennewell 1999). The time for a spacecraft to reach the peak altitude and the switching moment is delayed as the solar activity becomes stronger. For the case of maximum solar activity (Fig. 6), the spacecraft raises its altitude for about 2/3 of the operation time, and then drops rapidly for about 1/3 of the operation time owing to the high atmospheric density. In contrast, when solar activity is weak (Fig. 8), a spacecraft reaches the peak altitude at about 1/4 of the operation time, and then descends slowly for the remaining operation time. Fuel consumption for the case of maximum solar activity is about three times larger than that for minimum solar activity (Table 4).

Table 5 shows optimization results with different maneuver periods. Fuel consumption increases with the maneuver period, but this increase is not proportional. For example, the fuel consumption for 5 days is less than that for 1 day multiplied by 5. This is because a spacecraft reaches higher altitude where atmospheric density is lower when the maneuver period is longer. KOMPSAT-2 collects panchromatic imagery at 1m resolution with Instantaneous Field of View (IFOV) 1.46 μm at an altitude of 685 km. Based on the IFOV of KOMPSAT-2, Ground Sampling Distance (GSD) is calculated using the relation between GSD and altitude (Park et al. 2008). GSD could be improved to be under 0.5 by lowering the altitude of spacecraft.

Fig. 9 shows simulation results considering the *J*2 effect with atmospheric drag. Orbit inclination was set as 45 deg. A periodic change in altitude of about 13 km occurred due to the effect of *J*2. The time histories of longitudinal and latitudinal steering angles indicate that the thrust is applied

Table 4. Comparison between results of pseudospectral and combined methods for solar activity

Solar Activity	Maximum		Mean		Minimum	
Optimization Method	PS	Combined	PS	Combined	PS	Combined
Fuel Consumption(kg)	2.689	2.666	1.730	1.718	0.9433	0.878
Peak Altitude(km)	303.815	304.027	304.256	304.574	303.213	303.423
Final Altitude(km)	299.884	299.893	299.899	299.861	299.912	299.657
Switching Time(hr)	-	16.271	-	10.488	-	5.360
Atmospheric Density(kg/m3)	5.189e-11		3.379e-11		1.833e-11	

Table 5. Simulation results of combined method with maneuver period

Maneuver Period(day)	1	3	5	7
Fuel Consumption(kg)	1.718	4.671	7.422	9.356
Peak Altitude(km)	304.574	313.289	322.269	329.271
Final Altitude(km)	299.861	299.337	300.745	298.993
Switching Time(hr)	10.488	28.510	45.304	57.107
GSD(m)	0.445	0.457	0.471	0.481

Table 6. Simulation results of combined method with J_2 perturbation

Perturbation	Drag Only	Including J_2
Fuel Consumption (kg)	1.729	2.235
Peak Altitude (km)	304.569	304.658
Final Altitude (km)	299.859	300.047
Switching Time (hr)	10.552	13.638

along the direction of velocity vector. Table 6 confirms that a spacecraft uses about 30% more fuel when *J*2 perturbation is active, and thus it has remarkable effect on fuel-optimality of LEO spacecrafts.

5. CONCLUSION

Pseudospectral and shooting methods were combined to optimize the fuel consumption for altitude maintenance of spacecrafts at 300 km circular orbits where atmospheric drag is sufficiently strong to cause orbital decay. Based on the physical characteristics of KOMPSAT-2, simulations showed that a satellite ascended with full thrust at the early stage and then descended with null thrust. While the thrust profile was similar to bang-off, it was difficult to precisely determine the switching time by using only a pseudospectral method. As an attempt to precisely determine the switching time and its associated optimal thrust history, a shooting method was employed with its initial guess obtained from a solution using the pseudospectral method. By analyzing the results with solar activity, fuel consumption during the maximum solar activity was found to be three times more than that during the minimum solar activity. This implies that the solar activity cycle is a critical factor while designing a LEO mission. Furthermore, fuel consumption was reduced when the maneuver period of satellites was increased. This is possible because with extended maneuver periods, satellites reach higher altitudes where the atmospheric drag

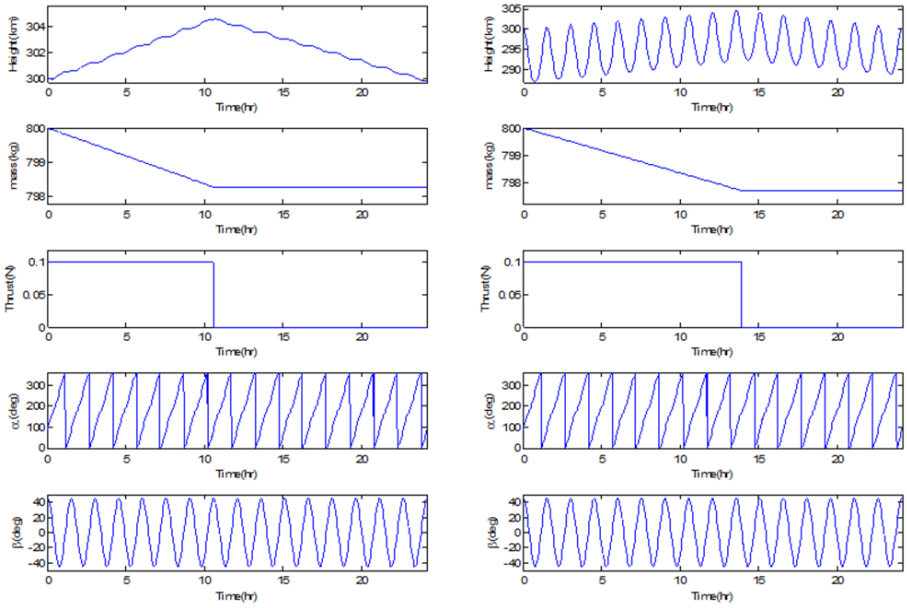

Fig. 9. Time histories of altitude, mass, thrust, and longitudinal/latitudinal steering angles obtained using combined method; air drag only (left) and active J2 effect (right).

is relatively weak. For the case considering $J2$ perturbation with drag, more fuel was used to maintain the altitude than for the case considering only drag; $J2$ perturbation has a remarkable effect on LEO spacecrafts, and should be taken into account for a more realistic mission design.

The overall hybrid process proposed in this paper can provide a robust, efficient, and precise fuel-optimal solution for various cases of satellite maneuvers.

ACKNOWLEDGMENTS

This work was supported by the Global Surveillance Research Center (GSRC) program funded by the Defense Acquisition Program Administration (DAPA) and Agency for Defense Development (ADD).

REFERENCES

Elnagar G, Kazemi MA, Razzaghi M, The Pseudospectral Legendre Method for Discretizing Optimal Control Problems, IEEE Trans. Autom. Control 40, 1793-1796 (1995). http://dx.doi.org/10.1109/9.467672

Halbach LE, A Numerical Study of Fuel-Optimal Low-Earth-Orbit Maintenance, Master Dissertation, Naval Postgraduate School (2000).

Jo JH, Park IK, Choe NM, Choi MS, The Comparison of the Classical Keplerian Orbit Elements, Non-Singular Orbital Elements (Equinoctial Elements), and the Cartesian State Variables in Lagrange Planetary Equations with J2 Perturbation: Part I, J. Astron. Space Sci. 28, 37-54 (2011). http://dx.doi.org/10.5140/JASS.2011.28.1.037

Kennewell J, Satellite Orbital Decay Calculations, IPS Radio and Space Services, The Australian Space Weather Agency, Sydney, Australia (1999).

Kim K, Current Status and Future Plan of Development of High-Resolution Earth-Observing Optical Satellites, Study on Aeronautical Industry, 65-85 (2013).

Kim K, Fuel Optimization for Altitude Maintenance of Low-Earth-Orbit (LEO) Spacecraft by Combining Direct and Indirect Methods, Master Dissertation, Yonsei University (2014).

Kluever CA, Pierson BL, Optimal Low-Thrust Three-Dimensional Earth–Moon Trajectories, J. Guid. Control Dyn. 18, 830–837 (1995). http://dx.doi.org/10.2514/3.21466

MathWorks, fmincon [Internet] cited 2015a, available from: http://kr.mathworks.com/help/optim/ug/fmincon.html

MathWorks, fsolve [Internet] cited 2015b, available from: http://kr.mathworks.com/help/optim/ug/fsolve.html

Park C, Necessary Conditions for the Optimality of Singular Arcs of Spacecraft Trajectories Subject to Multiple Gravitational Bodies, Adv. Space Res. 51, 2125-2135 (2013). http://dx.doi.org/10.1016/j.asr.2013.01.005

Park J, Moon YJ, Kim KH, Cho KS, Kim HD, et el., Drag Effect of KOMPSAT-1 during Strong Solar and Geomagnetic Activity, J. Astron. Space Sci. 24, 125-134 (2007). http://dx.doi.org/10.5140/JASS.2007.24.2.125

Park YJ, Park SY, Kim YR, Choi KH, Fuel Optimization for Low Earth Orbit Maintenance, J. Astron. Space Sci. 25, 167-180 (2008). http://dx.doi.org/10.5140/JASS.2008.25.2.167

Pontryagin LS, Mathematical Theory of Optimal Processes (CRC Press, New York, 1987).